with dry pyridine (py), followed by washing with dichloromethane, gave a quantitative yield of a green derivative $[Cu_3(TMA)_2(py)_3]_n \cdot 0.5py \cdot 2H_2O$ (*22*). Its x-ray diffraction pattern is similar to that of HKUST-1 in *d*-spacing and line shape, demonstrating that chemical functionalization can be achieved without a loss of structural integrity.

Although the resulting polymer $[Cu_3(TMA)_2(py)_3]_n$ cannot be obtained by a direct treatment of Cu(II) salts with TMA in pyridine solution (*23*), the use of either DMF or dimethylsulfoxide (DMSO) as the crystallizing solvent affords phase-pure solids that are isostructural with HKUST-1. These can be formed at RT in >80% yield and in multigram quantities. These solids still possess axial aqua ligands but contain channel DMF/DMSO and water (*24*). How such polar organic solvents play a structure-directing role in the formation of the tetracarboxylate moieties remains to be established, although changes in both solution speciation and product solubilities are probably involved.

Finally, the replacement of Cu by more oxophilic metals (Os_2 and others) in the framework of HKUST-1 should help achieve thermal stabilities in excess of 300°C. A TGA study of anhydrous [Er(TMA)] (*25*), which we have recently synthesized hydrothermally, shows no weight loss up to 500°C. Other metal substitutions may allow the introduction of redox centers {Ru(II)-Ru(III)}, the incorporation of catalytic sites (Rh_2), or a switch from neutral to charged frameworks {Re(III)-Re(III)}.

References and Notes

1. X. Bu, P. Feng, G. D. Stucky, *Science* **278**, 2080 (1997).
2. M. E. Davis, *Acc. Chem. Res.* **26**, 111 (1993); O. E. Akporiaye, *J. Chem. Soc. Chem. Commun.* **1994**, 1711 (1994); M. W. Anderson *et al.*, *Nature* **367**, 347 (1994); P. Feng, X. Bu, S. H. Tolbert, G. D. Stucky, *J. Am. Chem. Soc.* **119**, 24987 (1997).
3. S. T. Wilson, B. M. Lok, C. A. Messina, T. R. Cannon, E. M. Flanigen, *J. Am. Chem. Soc.* **104**, 1146 (1982); P. Y. Feng, X. H. Bu, G. D. Stucky, *Nature* **388**, 735 (1997).
4. B. F. Abrahams, B. F. Hoskins, D. M. Michail, R. Robson, *Nature* **369**, 727 (1994); M. Fujita, Y. J. Kwon, S. Washizu, K. Ogura, *J. Am. Chem. Soc.* **116**, 1151 (1994).
5. O. M. Yaghi, G. Li, H. Li, *Nature* **378**, 703 (1995); O. M. Yaghi, C. E. Davis, G. Li, H. Li, *J. Am. Chem. Soc.* **119**, 2861 (1997).
6. R. W. Gable, B. F. Hoskins, R. Robson, *J. Chem. Soc. Chem. Commun.* **1990**, 1677 (1990); T. Soma, H. Yuge, T. Iwamoto, *Angew. Chem. Int. Ed. Engl.* **33**, 1665 (1994); L. Carlucci, G. Ciani, D. M. Proserpio, A. Sironi, *J. Am. Chem. Soc.* **117**, 4562 (1995); G. B. Gardner, D. Venkataraman, J. S. Moore, S. Lee, *Nature* **374**, 792 (1995); S. R. Batten, B. F. Hoskins, R. Robson, *J. Am. Chem. Soc.* **117**, 5385 (1995); B. F. Abrahams, S. R. Batten, H. Hamit, B. F. Hoskins, R. Robson, *Chem. Commun.* **1996**, 1313 (1996); A. J. Blake *et al.*, *ibid.* **1997**, 1005 (1997); A. J. Blake *et al.*, *ibid.*, p. 2027; C. J. Kepert and M. J. Rosseinsky, *ibid.* **1998**, 31, (1998).
7. S. Subramanian and M. Zaworotko, *Angew. Chem. Int. Ed. Engl.* **34**, 2127 (1995).
8. R. Pech and J. Pickardt, *Acta Crystallogr.* **C44**, 992 (1988).
9. S. S.-Y. Chui and I. D. Williams, *ibid.* **C55**, 194 (1999).
10. S. O. H. Gutschke, A. M. Z. Slawin, P. T. Wood, *Chem. Commun.* **1996**, 823 (1996).
11. Crystals of $[Mn(TMA\text{-}H_2)_2(H_2O)_4]$ were formed by layer diffusion of ethanolic $[TMA\text{-}H_3]$ into aqueous $Mn(OAc)_2$ at RT. The monoclinic crystal system data are as follows: unit cell edges are a = 5.178(2) Å, b = 13.127(3) Å, and c = 15.142(3) Å; interaxial angle β = 97.74(2)°; and cell volume V = 1019(1) Å^3.
12. In a typical synthesis, 1.8 mM of cupric nitrate trihydrate was heated with 1.0 mM of trimesic acid ($TMA\text{-}H_3$) in 12 ml of 50:50 H_2O:EtOH (EtOH, ethyl alcohol) at 180°C for 12 hours in a Teflon-lined 23-ml Parr pressure vessel. This gave turquoise crystals up to dimensions of 80 μm in ~60% yield along with Cu metal and Cu_2O. Single-crystal x-ray analysis of the turquoise crystals (HKUST-1) was carried out with a Siemens diffractometer that was equipped with a SMART charge-coupled device.
13. Crystal data for HKUST-1 were measured as follows: $C_{18}H_{12}O_{15}Cu_3$, relative molecular mass M_r = 658.9, cubic crystal system, space group *Fm-3m*, a = 26.343(5) Å, V = 18,280(7) Å^3, formula units per cell Z = 16, density D_x = 0.96 g cm^{-3}, conventional discrepancy index R = 5.99, and weighted $wR2$ = 16.78; for 43 least-squares parameters and 853 reflections, diffraction angle 2Θmax = 50°. The structure was refined with SHELXL. A full description of the x-ray analysis is available at www.sciencemag.org/feature/data/986116.shl. The coordinates are on deposit with the Cambridge Structural Database, deposit number 112954.
14. F. A. Cotton, Z. C. Mester, T. R. Webb, *Acta Crystallogr.* **B30**, 2768 (1974); A. B. Brignole and F. A. Cotton, *Inorg. Synth.* **13**, 81 (1972).
15. P. Ceccherini, M. Curini, M. C. Marcotullio, O. Rosati, *Tetrahedron* **47**, 7403 (1991).
16. D. W. Breck, *Zeolite Molecular Sieves* (Kreiger, Malabar, FL, 1974), p. 48; *ibid.*, p. 625. The BET data are available at www.sciencemag.org/feature/data/986116.shl.
17. M. Fujita *et al.*, *Angew. Chem.* **37**, 2082 (1998); M. Fujita and K. Ogura, *Bull. Chem. Soc. Jpn.* **69**, 1471 (1996).
18. B. F. Abrahams, S. R. Batten, H. Hamit, B. F. Hoskins, R. Robson, *Angew. Chem. Int. Ed. Engl.* **35**, 1690 (1996).
19. Lattice expansion occurred in a family of Cu polymers containing N,N′ donor bridges [S. Katawa *et al.*, *Inorg. Chem.* **35**, 4449 (1996); S. Kitagawa, paper presented at the 1st International Conference on Inorganic Materials, Versailles, 16 to 19 September 1998].
20. H. Li, M. Eddaoudi, T. L. Groy, O. M. Yaghi, *J. Am. Chem. Soc.* **120**, 8571 (1998).
21. TGA results for HKUST-1 gave weight loss Δw = –28.2% from 25° to 120°C (–13 H_2O), thermal stability from 120°C to 250°C, and Δw = –25.4% from 250° to 400°C (–CO_2 and others). Further heating to 800°C resulted in a mixture of CuO and glassy C as final products. TGA curves are available at www.sciencemag.org/feature/data/986116.shl.
22. The analytical and calculated (in parentheses) data for $[Cu_3(TMA)_2(py)_3] \cdot 0.5(py) \cdot 2H_2O$ are as follows: C, 43.54% (46.48%); H, 3.54% (3.01%); and N, 5.52% (5.30%). TGA showed Δw = –3.9% from 25° to 120°C and Δw = –54.2% from 120° to 400°C (–py, –CO_2, and others).
23. A 2D network polymer $[Cu_3(TMA)_2(py)_9] \cdot 3(py) \cdot 3H_2O$ (space group *R-3c*, a = 19.142(5) Å, c = 42.64(1) Å, and V = 13,532 Å^3) was formed with large 48-membered rings of six individual Cu atoms and six TMA groups.
24. Analysis for the DMF product gave the best formulation as $[Cu_3(TMA)_2(H_2O)_3] \cdot 2.5(DMF) \cdot 2.5(H_2O)$, on the basis of combined chemical and thermal gravimetric analyses. The analytical and calculated (in parentheses) data are as follows: C, 34.6% (34.5%); H, 3.42% (3.89%); N, 4.01% (3.95%); Δw = –11.4% from 25° to 120°C (H_2O loss); and Δw = –48.6% from 150° to 400°C (DMF and CO_2 loss). Variable-temperature single-crystal studies of the DMSO derivative showed no bound DMSO at RT; heating up to 200°C produced intensity changes due to solvent loss (reflection 222 increases in intensity and reflection 400 decreases). Cooling to RT resulted in a general reversal of these trends.
25. Anhydrous [Er(TMA)] was synthesized hydrothermally at 180°C in a manner similar to the synthesis of HKUST-1; TGA under N_2 produced Δw = <–1% from 25° to 500°C and Δw = –45.7% from 500° to 650°C, corresponding to decarboxylation.
26. We are grateful to the Research Grants Council of Hong Kong (RGC grants 6148-97P and 6061-98P) and the Advanced Materials Research Institute (AMRI-HKUST) for financial support and to J. Zheng and A. Siu for technical assistance.

27 October 1998; accepted 4 January 1999

Direct Evidence for R^- Rotons Having Antiparallel Momentum and Velocity

M. A. H. Tucker and A. F. G. Wyatt*

Experimental evidence is presented that shows that the momentum of a R^- roton (a particle-like excitation in liquid helium-4) is antiparallel to its velocity. Although this is anticipated from the negative slope of the dispersion curve for these excitations, it has only been possible to test since the development of a source of ballistic R^- rotons. The backward refraction of the quantum evaporation process, which is the signature of antiparallel momentum and velocity, is observed.

Particles in free space obey Newtonian laws of motion at low speeds and relativistic laws at high speeds. The momentum $\mathbf{p}$ and velocity $\mathbf{v}$ of such a particle are connected by an equation of the form $\mathbf{p} = m\mathbf{v}$, and because mass (m) is always a positive quantity, $\mathbf{p}$ and $\mathbf{v}$ are parallel. Particles that move in a medium do not necessarily have $\mathbf{p}$ parallel to $\mathbf{v}$ because the momentum is a composite quantity involving both the particle and the reaction of the medium to its motion. Liquid ^4He at temperatures $T < 2.1$ K has particle-like

---

School of Physics, University of Exeter, Stocker Road, Exeter EX4 4QL, UK.

*To whom correspondence should be addressed.

excitations called R^- rotons that are expected to have **p** antiparallel to **v**. Here we describe an experiment that shows that this is indeed the case. This property is interesting not only because of its rarity but also because it leads to nonintuitive scattering behavior. This behavior can be illuminated by an analogy. Consider a tennis ball that has its momentum antiparallel to its velocity. When the approaching ball is hit with a racquet, the ball's direction is reversed as usual but its speed is reduced and the racquet does not recoil but accelerates forward (*1*). It is the unusual scattering behavior of R^- rotons at the free liquid surface that gives an unambiguous method of detecting the relative orientation of **p** and **v**.

Theoretically, **p** and **v** are expected to be antiparallel for R^- rotons because of the shape of the energy-momentum (dispersion) relation $\varepsilon(p)$. Landau (*2*) suggested the correct form of $\varepsilon(p)$ for excitations in superfluid ^{4}He, in which $T < 2.1$ K. This dispersion curve was first measured (*3, 4*) with neutron scattering. $\varepsilon(p)$ increases from $\varepsilon(p = 0) = 0$ to a local maximum at p_{maxon}, dips to a local minimum (the roton minimum) at p_0 with energy Δ, and then rises asymptotically to a limiting energy of 2Δ (*5*). The values of p_0 and Δ are $p_0/\hbar = 1.925 \times 10^{10}\ m^{-1}$ and $\Delta/k_B = 8.61$ K ($\hbar$, Planck's constant/2π; k_B, Boltzmann constant) (*6*). Excitations with $p < p_{\text{maxon}}$ are nearly pure propagating density fluctuations and are called phonons. Excitations with $p > p_{\text{maxon}}$ are called rotons and involve superfluid flow as well as density fluctuations. A roton that has $p > p_0$ is called a R^+ roton because the dispersion curve here has a positive gradient, and similarly a roton that has $p_{\text{maxon}} < p < p_0$ is called a R^- roton because the gradient is negative.

The velocity of a particle is given by the gradient $d\varepsilon/dp$ at the point (ε, p) on the dispersion curve. An object in free space has $\varepsilon = p^2/2m$ at nonrelativistic speeds and $\varepsilon^2 = c^2p^2 + m^2c^4$ at relativistic speeds, so $d\varepsilon/dp > 0$; that is, its dispersion curve has positive gradient and its velocity is therefore parallel to its momentum. In superfluid ^{4}He, however, $d\varepsilon/dp < 0$ for positive p in the interval $p_{\text{maxon}} < p < p_0$, so theoretically the velocity of a R^- roton should be antiparallel to its momentum. This also implies that if the energy of a R^- roton is increased, its momentum decreases.

There are few techniques available to measure roton properties. Although neutron scattering can measure ε and p, it is unable to measure the velocity and so cannot give information about the relative orientation of **p** and **v**. However, in a quantum evaporation experiment both **p** and **v** can be measured, so we can determine whether the momentum of a R^- roton is antiparallel to its velocity.

To perform the quantum evaporation measurement, it is necessary for the R^- roton to have a mean free path that is longer than the distance from the source to the free liquid surface so that the angle of incidence is well defined. The shape of the dispersion curve in the R^- region indicates that spontaneous decay of a R^- roton by phonon or roton emission is forbidden by energy and momentum conservation. Scattering from thermal excitations is made negligible by the use of low liquid temperatures, and scattering with other rotons emitted by the source can also be made negligible by limiting the flux. Time-of-flight measurements show that long R^- roton lifetimes can be achieved (*7*). The rotons are collimated into a beam directed at the free liquid surface. The velocity of the roton points toward the surface, and the modulus of the velocity is found from the time of flight. We use the interaction with the free liquid surface to show that the momentum of a R^- roton points back along the path toward the source. At the surface, the R^- roton scatters into a free atom state above the liquid; that is, the roton disappears and a free atom is created. In this process, energy and the component of momentum parallel to the surface are conserved. This latter condition arises from the translational invariance of the free liquid surface. The conservation laws are

$$\varepsilon = E_B + \frac{p_A^2}{2m} \tag{1}$$

$$p \sin\theta = p_A \sin\phi \tag{2}$$

where ε is the energy of the incident roton with momentum p, p_A is the momentum of the evaporated atom, E_B is the binding energy of the atoms to the liquid, and m is the mass of an atom. The path of the R^- roton makes an angle θ to the vertical and ϕ is the angle of the atom path relative to the vertical. These conservation laws (*8, 9*) have been verified with the use of phonons and R^+ rotons in quantum evaporation measurements (*10–12*).

The angle ϕ of the evaporated atom can be derived from Eqs. 1 and 2 and is given by

$$\sin\phi = \frac{p \sin\theta}{\sqrt{2m(\varepsilon - E_B)}} \tag{3}$$

The denominator has the dominant effect, so we see that for rotons of higher energy the evaporated atom is ejected at a smaller angle to the normal. This angular dispersion of quantum evaporation allows us to perform spectroscopy on the roton distribution. For a R^+ roton, ϕ is positive so the atom path has the same horizontal direction as the path of the roton. However, if p is negative then the angle ϕ is negative, so atoms evaporated by R^- rotons should be refracted backward (Fig. 1). So we need only show this direction of the evaporated atom to demonstrate that **p** is antiparallel to **v**.

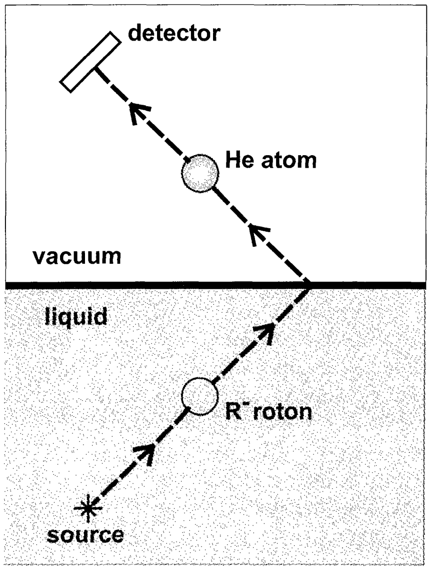

Fig. 1. Schematic of quantum evaporation showing the negative refraction of the R^- roton evaporation path at the free liquid surface of superfluid ^{4}He. No horizontal momentum is imparted to the surface, so the atom has the same horizontal momentum as the R^- roton. This stems from the translation invariance of the surface.

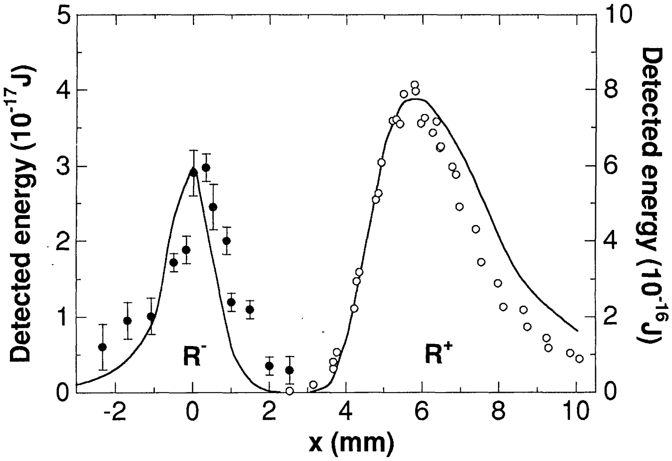

Fig. 2. The flux of evaporated ^{4}He atoms as a function of the horizontal position x of the detector. The detector is 3 mm above the liquid surface and the source is 9 mm below the surface at $x = 0$. The open circles correspond to evaporation by R^+ rotons (energy scale at right). The error bars are comparable with, or smaller than, the circles. The solid circles correspond to evaporation by R^- rotons (energy scale at left). The solid line is the numerical simulation of the experiment for evaporation by R^- rotons (left) and R^+ rotons (right). The effective temperature of the roton distribution that fits best is 1.0 K.

A fast source of R$^-$ rotons that enables this experiment to be performed has recently been developed (*13*). It is based on collisions between R$^+$ rotons as follows

$$\begin{aligned} R^+ + R^+ &\rightarrow R^+ + R^- \\ R^+ + R^+ &\rightarrow R^- + R^- \end{aligned} \tag{4}$$

The source consists of two parallel metal films that form a narrow open-sided cavity containing liquid ^{4}He. The two metal films are heated simultaneously with a short pulse of current, injecting R$^+$ rotons and low-energy phonons into the cavity. R$^-$ rotons are not injected by these heated films (*14*) but are created when the R$^+$ rotons interact. The pulse of R$^+$ and R$^-$ rotons emitted from the cavity is short enough for time-of-flight measurements. This information gives an independent check that we are observing the effects of ballistic rotons and not spurious reflections.

To measure the quantum evaporation angle, the emitted rotons need to be collimated. We do this with horizontal semicircular slits so that the beam has the shape of the surface of a half cone. The source is ~9 mm below the liquid surface, and $\theta = 16.5°$ with a beam profile full width at half maximum of 7.5°. Atoms from R$^-$ rotons should be refracted backward and converge several millimeters above the liquid surface, vertically above the source. This collimation arrangement enhances the R$^-$ roton evaporation signal at a detector placed here (*15*). The detector can be moved horizontally so that the divergent beam of atoms from the R$^+$ rotons can also be detected for comparison.

The detector is 3 mm above the liquid surface. The energy deposited on the detector as a function of its horizontal position x (Fig. 2) is clearly composed of two separate components: maxima at $x \sim 0$ (directly above the roton source) and at $x \sim 6$ mm, with a minimum of almost zero at $x \sim 2.5$ mm. This spatial distribution of atoms is that expected from a beam containing R$^-$ and R$^+$ rotons. The peak on the left comes from R$^-$ rotons and the peak on the right from R$^+$ rotons. The times of flight support this identification. The result clearly shows the negative refraction of atom paths relative to R$^-$ roton paths, thus demonstrating that the momentum and velocity of a R$^-$ roton are antiparallel.

To make a quantitative comparison with theory we have made a computer simulation. A Monte Carlo procedure selects a roton from a thermal distribution at the source and follows it through the geometry of the collimation to the surface. An atom is liberated according to Eqs. 1 and 2, and a test is made of whether the atom hits the bolometer. For a roton spectrum with an effective temperature of 1 K, the simulation reproduces the main features of the measurements very well (Fig. 2). The remaining difference is most likely due to the evaporation probability being momentum dependent; in the simulation we took this probability to be constant because current theories of quantum evaporation do not agree on the momentum dependence (*16–18*).

We are only just beginning to understand the true nature of rotons. Now that beams of R$^-$ rotons can be created, it should be possible to scatter them from R$^+$ rotons and probe their internal structure.

References and Notes

1. Assume that the kinetic energy ε as a function of momentum p of this hypothetical ball, mass m, is $\varepsilon = (p - p_0)^2/2m$ where $p_0 > 0$ and $0 < p < p_0$. The Newtonian racquet is assumed, as usual, to have a mass larger than that of the ball.
2. L. D. Landau, *J. Phys. Moscow* **11**, 91 (1947).
3. H. Palevsky, K. Otnes, K. E. Larsson, *Phys. Rev.* **112**, 11 (1958).
4. J. L. Yarnell, G. P. Arnold, P. J. Bendt, E. C. Kerr, *ibid.* **113**, 1379 (1959).
5. H. R. Glyde, M. R. Gibbs, W. G. Stirling, M. A. Adams, *Europhys. Lett.* **43**, 422 (1998).
6. W. G. Stirling, in *Proceedings of the Second Internal Conference on Phonon Physics*, J. Kollár, N. Kroó, N. Menyhárd, T. Siklós, Eds. (World Scientific, Singapore, 1985), pp. 829–835.
7. M. A. H. Tucker and A. F. G. Wyatt, *J. Low Temp. Phys.* **113**, 615 (1998).
8. P. W. Anderson, *Phys. Lett.* **29A**, 563 (1969).
9. M. W. Cole, *Phys. Rev. Lett.* **28**, 1622 (1972).
10. M. J. Baird, F. R. Hope, A. F. G. Wyatt, *Nature* **304**, 325 (1983).
11. F. R. Hope, M. J. Baird, A. F. G. Wyatt, *Phys. Rev. Lett.* **52**, 1528 (1984).
12. M. Brown and A. F. G. Wyatt, *J. Phys. Condens. Matter* **2**, 5025 (1990).
13. M. A. H. Tucker and A. F. G. Wyatt, *J. Low Temp. Phys.* **110**, 455 (1998).
14. When the cavity roton source was replaced by a single heater, there was no evidence for quantum evaporation signals from R$^-$ rotons.
15. H. Baddar, D. O. Edwards, T. M. Levin, M. S. Pettersen, *Physica* B **194-6**, 513 (1994).
16. F. Dalfovo, A. Fracchetti, A. Lastri, L. Pitaevskii, S. Stringari, *Phys. Rev. Lett.* **75**, 2510 (1995).
17. C. E. Campbell, E. Krotscheck, M. Saarela, *ibid.* **80**, 2169 (1998).
18. M. B. Sobnack and J. C. Inkson, *Phys. Rev.* B **56**, R14271 (1997).

19. We thank the Engineering and Physical Sciences Research Council for financial support, M. Gear for making the apparatus, and C. D. H. Williams for advice on the electronic detection system. We benefited from general discussions with F. Dalfovo, M. Guilleumas, E. Krotscheck, M. B. Sobnack, S. Stringari, and C. D. H. Williams.

2 December 1998; accepted 18 January 1999

A Processive Single-Headed Motor: Kinesin Superfamily Protein KIF1A

Yasushi Okada and Nobutaka Hirokawa*

A single kinesin molecule can move "processively" along a microtubule for more than 1 micrometer before detaching from it. The prevailing explanation for this processive movement is the "walking model," which envisions that each of two motor domains (heads) of the kinesin molecule binds coordinately to the microtubule. This implies that each kinesin molecule must have two heads to "walk" and that a single-headed kinesin could not move processively. Here, a motor-domain construct of KIF1A, a single-headed kinesin superfamily protein, was shown to move processively along the microtubule for more than 1 micrometer. The movement along the microtubules was stochastic and fitted a biased Brownian-movement model.

A single kinesin molecule has two heads or motor domains (*1*) and moves processively (*2–4*), taking more than 100 steps before detaching from a microtubule (MT). The two-headed structure is assumed to be essential for processive movement, because engineered single-headed or monomeric molecules have motor activity but are not processive, whereas dimeric constructs have high processivity (*4–9*). The prevailing hypothesis for the mechanism of processive movement is the "walking model" (*2, 10*), in which one head anchors the molecule to the MT while the other moves to the next binding site on the MT. Thus, a single-headed molecule is not expected to move processively because the molecule is not anchored while it moves to the next binding site.

A monomeric kinesin superfamily protein, KIF1A, which has only one motor domain, supports MT gliding at ~1.2 μm/s (*11*). It remains unresolved whether this naturally single-headed KIF is processive or not. A conventional, very low motor density MT gliding assay and a single-motor motility assay with fluorescently labeled full-length KIF1A protein suggested that it is processive (*12*). However, the results were very variable, possibly because of the instability or heterogeneity of the full-length KIF1A recombinant protein. Thus, to overcome these problems, we produced a KIF1A motor-domain chimer-

---

Department of Cell Biology and Anatomy, Graduate School of Medicine, University of Tokyo, Hongo, Tokyo 113-0033, Japan.

*To whom correspondence should be addressed. E-mail: hirokawa@m.u-tokyo.ac.jp